Attenuation Correction in Dual-Wavelength Analyses

JOHN D. TUTTLE AND RONALD E. RINEHART

National Center for Atmospheric Research,[1] Boulder, CO 80307

(Manuscript received 5 February 1983, in final form 12 August 1983)

ABSTRACT

In using a dual-wavelength radar system to detect hail, erroneous positive hail signals can result because of the stronger attenuation of the shorter wavelength radar beam. We present a simple technique to correct for attenuation in dual-wavelength analyses. The technique makes use of an attenuation-reflectivity relationship of the form, $A = CZ_s^p$, where Z_s is the S-band reflectivity, C is a coefficient which is determined on a ray-by-ray basis, and p is the exponent, which is assumed to be a constant. In situations where rays of radar data contain a mixture of rain and hail, the attenuation-correction scheme can erroneously apportion more of the attenuation to hail regions rather than to rain regions. The scheme is modified to account for such situations.

1. Introduction

The attenuation of electromagnetic radiation by hydrometeors has long been a problem in the use of radar. The use of a dual-wavelength radar system to detect hail is no exception in that erroneous positive hail signals[2] can result because of the stronger attenuation of the shorter wavelength radar beam.

There have been numerous attempts in the past two decades to use dual-wavelength radars to detect hail, but thus far there have been few attempts to correct for attenuation. Jameson (1977) and Jameson and Heymsfield (1980) corrected for attenuation only at the lowest elevations by fitting a least squares, piecewise linear fit to the dips in their DWR data and subtracting this fit from the DWR to get hail signal. They found that attenuation was significant only below the melting level. In another approach, Eccles (1979) found the minima in the DWR along the radials of an elevation scan and fitted to them a smooth surface which monotonically increased with range. This surface was then subtracted from the DWR field to get the hail signal. Both approaches use the minima of the DWR in order to reduce the possibility of errors being caused by non-Rayleigh scatterers (i.e., hail).

In another hail detection study, Barge and Humphries (1980) used a polarization diversity, dual-wavelength radar system to distinguish among various types of hydrometeors. In their data analysis they carefully avoided areas where attenuation might be a problem.

Failure to account for attenuation can also lead to errors in the operations and evaluation of hail suppression experiments. Since the early 1960's, scientists in the Soviet Union have carried out numerous hail suppression experiments (Sulakvelidze, 1965). To know where to seed storms, they used a dual-wavelength radar system to find the locations of hail centers. In comparing the diameters of hailstones collected at the ground (after accounting for melting) with those calculated from dual-wavelength measurements, they found that the calculated diameters were systematically higher than the observed diameters (Sulakvelidze, 1968). They attributed this discrepancy to the attenuation of their 3.2 cm radar.

Because of the importance of attenuation in dual-wavelength analysis and the lack of work that has been done in correcting for it, there has been a need to investigate further the effects of attenuation and how to correct for it. We present here a simple technique to account for attenuation in dual-wavelength analyses. It is done on a ray-by-ray basis, takes little additional computing time and can be done on only one pass through the data.

2. Technique

The data used in this study were collected with the NCAR CP-2 dual-wavelength radar (10.7-cm and 3.2-cm wavelengths) located at Miles City, Montana, during the Cooperative Convective Precipitation Experiment (CCOPE) operated jointly by the National Center for Atmospheric Research and the Bureau of Reclamation during the summer of 1981. Data from storms on 11 July and 2 August were used in this study. Both storms were intense storms, having peak reflectivities of 75 dBZ, producing baseball-size and

[1] The National Center for Atmospheric Research is sponsored by the National Science Foundation.

[2] Dual-wavelength ratio or DWR is defined as the ratio of the radar reflectivity factor at the longer wavelength to that at the shorter wavelength and is usually expressed on a decibel scale. When the dual-wavelength ratio is corrected for attenuation, it is called "hail signal".

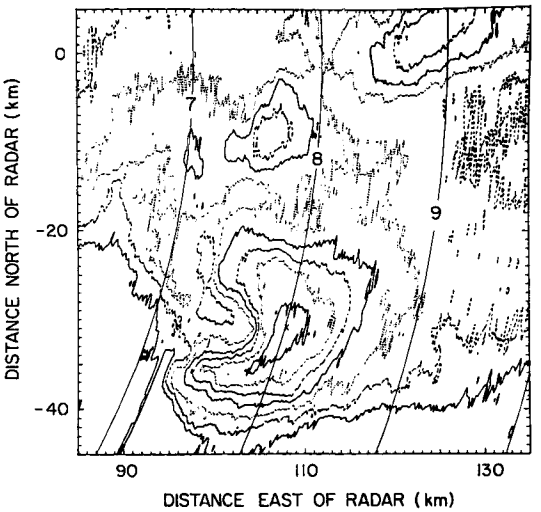

FIG. 1. S-band radar reflectivity field at 3.3° elevation for the 2011 MDT volume scan of the 11 July 1981 storm. Contours are at 10 dB intervals and start at 10 dBZ. The solid arcs give height (km) above mean sea level.

larger hail and lasting 4–6 hours. The 2 August storm also produced a possible tornado and had gust-front winds of 30 m s^{-1} (Wade, 1982). Figs. 1 and 2 show mid-level PPIs of each of these storms.

a. Calibration correction

In order to determine attenuation from dual-wavelength data it is first necessary to correct the data for any calibration, azimuth pointing, range and antenna beam pattern errors (Rinehart and Tuttle, 1981a, 1982a). The S-band radar was generally calibrated daily. The X-band radar, however, was calibrated only once during the CCOPE project. Thus there could well have been drifts in its receiver and/or transmitter during the season, resulting in changes in the calibration. Following the procedure introduced by Eccles (1975) and used by Jameson and Heymsfield (1980) and Rinehart and Tuttle (1982a), the X-band radar was calibrated with the S-band by looking at the differences in reflectivities at the edge of the storm nearest the radar. We found average S- minus X-band differences of −0.4 and −4.4 dB for 11 July and 2 August, respectively[3]. These average differences were then added to the X-band calibration to bring it into better agreement with the S-band data. In our data analysis, we defined the near and far edges of the storm to be where ten consecutive gates of X-band reflectivity were 10 dB above noise level.

b. Azimuth, range and time-to-independence errors

Using the sun's known azimuth as a standard, the pointing error beween the S- and X- band antennas was determined to be about 0.1° and hence could be neglected (Carbone, 1972, Rinehart and Tuttle, 1982a). Since the two antennas were mounted on the same pedestal, the pointing error should have remained nearly constant throughout the season. Using ground targets, range errors no larger than about 40 m were found for either 11 July or 2 August. Range errors of this magnitude are negligible.

Before any processing was done, a 3-gate running average was done on the S-band data in order to correct for any time-to-independence and receiver bandwidth differences in the two radars (Rinehart and Tuttle, 1982a).

c. Antenna beam pattern effects

In a dual-wavelength radar system, mismatched antenna beam patterns can produce erroneous positive or negative DWR (Rinehart and Tuttle, 1982a). In our attenuation–correction scheme (to be described in detail shortly), we use the differences in the S- and X-band reflectivity to determine X-band attenuation. Thus beam-pattern-produced erroneous DWR could lead to errors in estimating X-band attenuation. A new X-band antenna was put on the radar for the 1981 season; it resulted in a much better X-band beam pattern than with the old dual-wavelength system. We

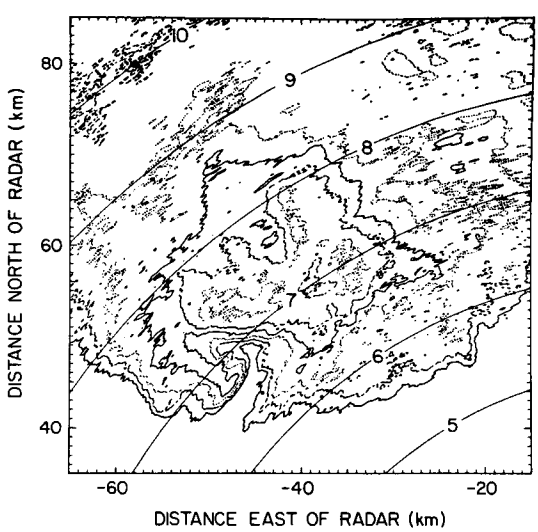

FIG. 2. As in Fig. 1, but for 2 August 1981 at 1704 MDT and 5.0° elevation.

[3] While the variation in the S- and X-band calibration difference between 11 July and 2 August is sizable, an examination of the data from several different CCOPE storm days showed little day-by-day variation. Days between 22 July and 4 August had calibration differences ranging from −4.8 to −4.1 dB and with the exception of one day, days between 9 June and 19 July had differences ranging from −1.4 to −0.4 dB. This indicates that a shift in the relative calibration of the S- and X-band systems occurred sometime between 19 July and 22 July with the first half of the field season having a relatively stable calibration and the second half having a different, but also stable, calibration.

ran our antenna beam pattern simulation program[4] using the new beam pattern measurements and the 11 July and 2 August data sets (Rinehart and Tuttle, 1982b). For both data sets, simulated negative hail signals no larger (i.e., more negative) than −0.2 dB were produced. There were, however, areas of positive hail signals as large as 8 or 9 dB. These occurred in regions of weak S-band reflectivity and generally in regions below X-band noise level in the real radar data. Since we used a threshold 10 dB above X-band noise level in our data processing, positive hail signals produced by mismatched beam patterns will generally not be a problem.

d. *Attenuation scheme*

Briefly, the attenuation-correction scheme looks at the difference (dB) between the logarithms of the S- and X-band reflectivities (DWR) on the far side of the storm away from the radar for each ray of data and assumes that this difference is the total attenuation that the X-band beam suffered in passing through the storm. The total attenuation is then apportioned according to the following equation and the DWR is correspondingly adjusted to correct for attenuation.

$$A = CZ_s^p, \tag{1}$$

where A is attenuation (dB km^{-1}), Z_s the S-band reflectivity (mm^6 m^{-3}), p a constant and C is a variable determined for each ray.

Now let us examine the attenuation scheme in more detail. First, looking at a single ray of S- and X-band data, a six-gate running average of the DWR is performed, following the suggestions of Jameson (1977). Then, using the average DWR data, the minimum value of the DWR in the last 2 km of storm (on the far side of the storm for each ray) is found. If the minimum DWR is zero or negative, i.e., the X-band reflectivity is equal to or larger than the S-band reflectivity, attenuation is calculated according to

$$A = 0.00048Z_s^{0.6}, \tag{2}$$

where the leading coefficient and the exponent are average values determined from the 11 July and 2 August data sets. The derivation of the leading coefficient and the exponent in Eq. (2) will be discussed in the next section. If the minimum DWR is positive, however, we proceed by summing the S-band reflectivities along the ray from the beginning to the end of the storm and use this cumulative S-band reflectivity and the minimum DWR value to determine the leading coefficient C in Eq. (1). In the actual calculations, Eq. (1) becomes $A_t = C\Sigma Z_s^p$ where A_t is the total attenuation (dB) through the storm (i.e., the logarithm of the S- and X-band reflectivity ratio on the far side of the storm). Once the coefficient C is determined, one starts back at the beginning of the storm and calculates the attenuation contributed at each individual range gate, i.e., the total attenuation is apportioned along the ray in proportion to the reflectivity at each point. By using the S-band reflectivity in the equation to calculate the X-band attenuation, we are assuming (as do all other authors) that the attenuation at S-band is negligible. Battan (1971) shows this to be a reasonable assumption.

To say that the minimum DWR at the far edge of the storm is equal to the X-band attenuation also assumes that there is no hail at the location of minimum DWR. While it is possible that such a situation could occur in nature, we feel reasonably comfortable that only rarely will this assumption be violated.

e. *Exponent in A–Z relationship*

The use of a constant exponent in the attenuation–reflectivity relationship is both reasonable and with precedent. An examination of published A–Z relationships (Battan, 1973; Eccles, 1979) reveals that for a given wavelength and temperature there are only moderate differences in the quoted exponents. Further, Eccles (1979) also assumed that the exponent could be held constant when he chose to adjust the leading coefficient of a modified A–Z relationship from Atlas and Ulbrich (1974) to force his precipitation totals determined from attenuation to agree with those predicted from S-band reflectivity.

Instead of using the exponent from an existing A–Z relationship, we chose to determine one based on the 11 July and 2 August data sets. We started by taking a ray of data through the storm and finding the attenuation between two data points separated by 10 gates along with the average S-band reflectivity between the points. The attenuation was calculated by

$$A = \left[10 \log\left(\frac{Z_{si+10}}{Z_{xi+10}}\right) - 10 \log\left(\frac{Z_{si}}{Z_{xi}}\right)\right] \Big/ \Delta r,$$

where A is the attenuation in dB km^{-1}, Z_s and Z_x are the S- and X-band reflectivities at the ith and ith + 10 gates and Δr is the distance in km between the ith and ith + 10 gates. This process was repeated for consecutive pairs of data points in the ray and for each ray of an elevation scan. As the processing was done, the attenuation values were accumulated in bins (2 dB wide) of average S-band reflectivity. At the end of an elevation scan, average attenuation values were calculated for each bin. It should be noted that in calculating the attenuation, care was taken to avoid regions of non-Rayleigh scatterers. This was done by

[4] The antenna beam pattern simulation program, which is described in detail in Rinehart and Tuttle (1982a), consists of taking a storm volume collected by the S-band radar and resampling the volume at each of the data points with the S- and X-band antenna beam patterns. The resampling was done by adding in the antenna-beam-pattern-weighted reflectivity from all points at the same range as the point being sampled. The S- and X-band beam patterns were determined by slowly scanning a radio tower (Rinehart and Tuttle, 1981b).

assuming an initial A–Z relationship, correcting the DWR for attenuation, and avoiding those regions where the resulting hail-signal was greater than 3 dB.

Figure 3 shows an example of the average attenuation plotted against the logarithm of the S-band reflectivity for 11 July data at an elevation of 0.5°. As expected, the attenuation increases essentially exponentially with reflectivity. On a log–log scale, i.e., $\log(A)$ versus $\log(Z_s)$, this becomes a linear curve. Taking the logarithm of Eq. (1) results in

$$\log(A) = \log(C) + p \log(Z_s).$$

A least-squares linear curve was fitted to the $\log(A)$–$\log(Z_s)$ data points (but only for those with $A > 0$) to obtain C and p. This procedure was repeated for several elevations both above and below the melting level and for both 11 July and 2 August data. The average exponents found were 0.648 and 0.456 for below and above the melting level, respectively. The attenuation above the melting level was less than below because of the presence of ice rather than liquid water.

Although we have distinguished here between the upper and lower levels of the storm and calculated two different powers, we will, in subsequent analyses, use a constant power for all regions of the storm. The power chosen was 0.6, being somewhat of a compromise between the two values. It will be shown in Section 3 that the attenuation–correction scheme is not very sensitive to the choice of the power.

The average leading coefficient found for the two datasets was 0.00048. This is the leading coefficient that is used for cases where the minimum DWR is zero or negative [Eq. (2)]. Eq. (2) will generally be applied only in weak reflectivity areas where there is no appreciable X-band attenuation. Hence, the choice of the leading coefficient is not very critical.

f. Handling hail

All of the preceeding discussion assumes that non-Rayleigh scatterers (i.e., hail) are not being detected by the radar. What happens when hail is present? Moderate to large-size hail (diameters > 2 cm) can produce S-band reflectivities in excess of 70 dBZ (Donaldson, 1960; Atlas and Ludlam, 1961), but the X-band attenuation in such hail regions can be considerably less than the attenuation in regions of somewhat weaker reflectivity containing rain only. By apportioning the attenuation according to S-band reflectivity, this attenuation–correction scheme could, in rays of data containing a mixture of rain and hail, erroneously apportion too much of the attenuation to the hail rather than to the rain.

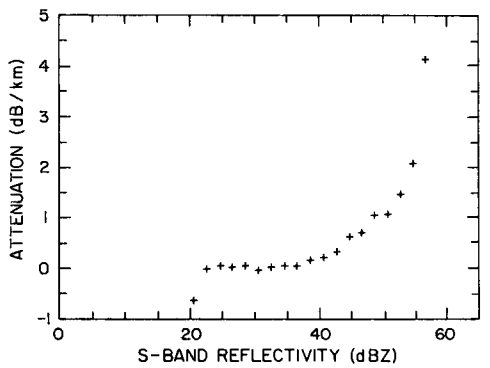

FIG. 3. The average attenuation (dB km^{-1}) as a function of S-band reflectivity (dBZ) at 0.5° elevation for the 2015 MDT volume scan of the 11 July 1981 storm. Least squares curve fitting was applied only for $A > 0$ dB.

To account for this problem, the attenuation–correction scheme was modified using an approach that combined the methods used by Jameson (1977) and Eccles (1979) and the method described above. Looking at a single ray of data, one first locates all the dips in the smoothed DWR data, starting at the far edge of the storm. Since attenuation has to increase monotonically with range, a dip closer to the radar has to be less than or equal to the next dip that was farther away in range. If a nearer dip is greater than the next farther one, it is not counted. The differences between consecutive pairs of these dips then represent the attenuation along segments of the ray. Then employing the same method as described in Section 2.d, the leading coefficient in Eq. (1) is found for each segment of the ray, and the attenuation is again apportioned according to S-band reflectivity. Utilizing the dips in the difference field helps eliminate using areas of non-Rayleigh scatterers in determining attenuation, and the resulting segmentation of the rays aids in apportioning more correctly the total attenuation between hail and non-hail areas.

3. Results and discussion

Figure 4 shows an example of applying the attenuation correction technique to a ray of data at a moderately high elevation angle in the 2 August 1981 storm. Curves A and B show the profiles of the logarithm of the S- and X-band reflectivities, respectively, through the storm. The S-band profile starts out below the X-band (the S-band receiver has a much lower minimum detectable signal and better overall sensitivity than the X-band) on the left, but as the storm is entered they are virtually the same. As the storm is penetrated further, the X-band signal is strongly attenuated. Curves C and D show the DWR (after the 6-gate smoothing) without correcting (C) and after correcting (D) for attenuation. The straight lines F, G and H represent +3, 0, and −3 dB of difference. Jameson and Heymsfield (1980) and Heymsfield *et al.* (1980) ignored hail signals between −3 and +3 dB to avoid problems caused by the well-known noisiness of the hail signal (Srivastava and Carbone, 1971 and Eccles, 1979). Curve E is the cumulative attenuation curve.

On the near side of the storm, the S- and X-band

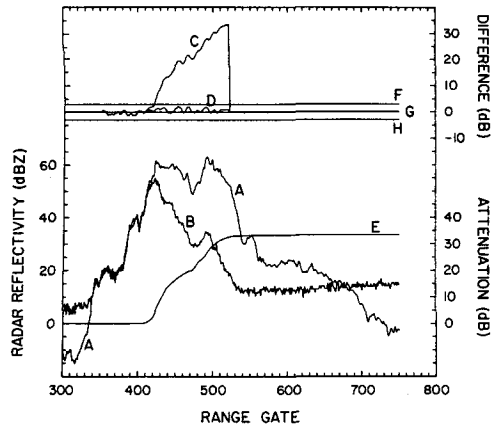

FIG. 4. S-band (curve A) and X-band (curve B) reflectivities along 327.4° azimuth and 6.1° elevation at 170451 MDT of the 2 August 1981 storm. Range gate 300 is at 45 km from the radar and gates are 150 m apart. The other curves are as follows: C) DWR smoothed over 6 gates; D) attenuation-corrected DWR, i.e., hail signal; E) cumulative attenuation; F), G) and H) are reference lines 3 dB above, at and 3 dB below zero hail signal.

reflectivity differences are near zero. On the far side, however, the total loss of the X-band signal approaches 34 dB. Reducing this curve (C) by the cumulative attenuation curve (E) produced the attenuation-corrected reflectivity difference curve (D). This curve is thus the hail signal through this part of the storm and is not significantly different from zero. The height in the storm of this region is around 8–9 km MSL which is far above the melting level (4.5 km). Thus, in this example, not correcting for attenuation would lead to significant errors in dual-wavelength analysis, even above the melting level.

Now let us consider the use of a constant power p in Eq. (1). Fig. 5 shows the same ray as Fig. 4 with 3 different attenuation-corrected curves superimposed on top of each other using values of p of 0.4, 0.6, and 0.8. The difference between the 0.4 and 0.8 curves is at the most only about 0.5 dB, so the curves are essentially indistinguishable. These differences would be even less for cases of less extreme attenuation. Thus, the choice of the constant power has little effect on the results of this attenuation-correction scheme.

Figure 6 shows a ray of data containing both hail and rain, and compares attenuation results using the original attenuation scheme described in Section 2.d (Fig. 6a) and the modified scheme using the dips (Fig. 6b). The ray of data is taken through the lower portion of the 2 August storm. The S-band reflectivity rises rather abruptly at the near edge of the storm to values over 70 dBZ and then drops off more slowly towards noise level on the far side. The X-band reflectivity also rises abruptly, but reaches a peak of only about 60 dBZ. After reaching the peak the X-band signal drops rapidly and reaches noise level long before the S-band signal does. The S- and X-band difference profile (C) reaches a peak of about 24 dB almost immediately at the near edge and then dips down to 10 dB before increasing again to around 35 dB on the far edge. Curve D (Fig. 6a), which results when applying the attenuation correction to curve C, shows a large negative hail signal of about −13 dB. Since theory predicts that negative hail signals no larger (no more negative) than about −4 dB can occur and the new antenna beam patterns no longer produce the large erroneous negative hail signals that the old system did (Rinehart and Tuttle, 1982b), there must be some other explanation for the −13 dB hail signal. Our interpretation for this is as follows. The path along the ray can basically be divided into two parts: a region of mostly hail followed by a region of mostly rain. At the front edge of the storm there is hail as is evident from the large S- and X-band difference and the high S-band reflectivity. In this region there is relatively little attenuation of the X-band signal (the X-band reflectivity rises to within about 8 dB of the S-band signal at the back of this region). After the X-band signal reaches its peak, it rapidly becomes attenuated even though the S-band reflectivity has dropped to below 60 dBZ. This would indicate that the beam has left the hail area and has entered an area of heavy rain, causing strong X-band attenuation[5].

Using the attenuation–correction scheme, we find a total attenuation of about 36 dB at the back edge of the storm for this ray. In Fig. 6a this total attenuation is apportioned to the S-band reflectivity; a majority of the attenuation is attributed to the 70 dBZ region of

[5] This interpretation as to the location of hail and rain is consistent with reports from ranchers in the Miles City area who observed the storm. Many of them reported large size hail (up to softball size) without rain first, followed by smaller hail mixed with rain and finally rain only (Wade, 1982). The storm at this time was to the northwest of the radar and was moving toward the east-southeast.

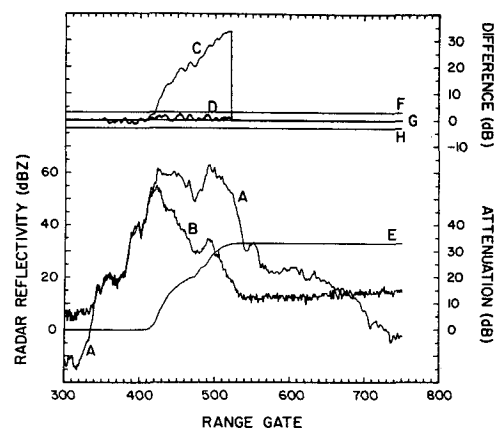

FIG. 5. As in Fig. 4 except that three S-minus-X attenuation corrected curves are superimposed on top of each other. These correspond to using values of power p of 0.4, 0.6 and 0.8. The differences are so small that the three curves almost appear as one curve.

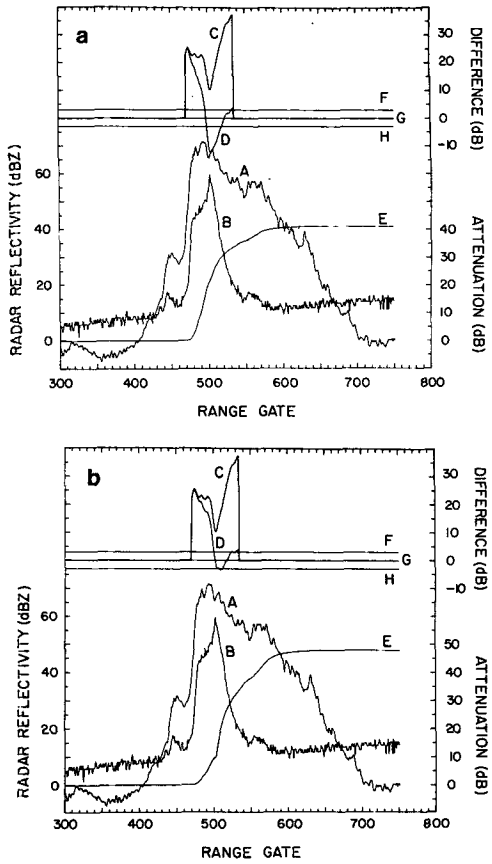

FIG. 6. A comparison of using (a) the attenuation-correction scheme described in Section 2d and (b) the modified scheme described in Section 3. The data are from the 318.76° azimuth and 0.6° elevation at 1703:13 MDT of the 2 August 1981 storm. The labeling of the curves is the same as in Fig. 4.

the storm. Hence, by the time the far side of the hail region is reached, there has already been 20 dB of attenuation when it should be considerably less. The result is to pull down the dip too far, giving a strong negative hail signal. Using the modified attenuation–correction (Fig. 6b), the ray was objectively broken up into two segments, the first segment being the mostly-hail region and the second the mostly-rain region. Now the hail region is producing only about 8 dB of attenuation while the rain is giving the majority of the attenuation. The peak value of the hail signal has not changed, but the overall size and strength of the region has increased, and the negative signal has disappeared.

Figure 7 shows an example of the integrated attenuation field which results when using this attenuation–correction technique. The plot corresponds to the reflectivity field of Fig. 2. The contour levels start at 3 dB of integrated attenuation and increase in increments of 3 dB. Thus, even at this height (6–8 km MSL), the total attenuation is in excess of 30 dB at some locations. The strongest attenuation is radially away from the two northern-most 60-dBZ cores (see Fig. 2). The southern-most 60 dBZ core shows considerably less attenuation than the northern ones. This is primarily due to the fact that the southern core has less radial extent than the northern ones.

Figure 8 shows examples of the DWR without (a) and with (b) applying the attenuation correction to the data set shown in Fig. 2. Fig. 8a shows extensive regions of S- and X-band reflectivity differences greater than 3 dB, but little reliance can be placed upon the results. After attenuation correction, however, more believable patterns of hail emerge. The strongest area of hail signal occurs in the southern core.

The data used in the examples shown above are from large intense storms causing strong X-band attenuation. These storms were chosen in order to investigate how the attenuation–correction scheme would handle cases of extreme X-band attenuation. In an earlier study, Rinehart and Tuttle (1982a) applied an earlier version of the attenuation–correction scheme to a more moderate storm (producing 5–6 dB of attenuation at mid-levels) with equally good results. Thus, this attenuation–correction scheme appears to handle adequately storms at both ends of the spectrum.

One final problem remains in this attenuation–correction scheme. Occasionally the attenuation is so severe that the X-band signal is reduced to noise level while the S-band signal is still quite strong. Fig. 9 shows an example of this from 11 July data. In this example, the X-band signal becomes attenuated so much that it falls below our X-band noise threshold before the beam passes through the 65-dBZ reflectivity core. In a 65 dBZ core there is likely to be hail; attempting to calculate attenuation in hail regions would certainly lead to erroneous results. Our assumption that there is no hail in the last 2 km of the storm would probably

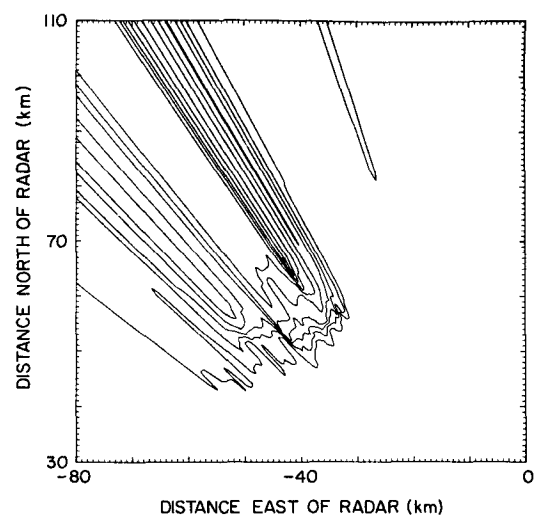

FIG. 7. Example of the integrated attenuation field produced by the attenuation-correction scheme at 5.0° elevation for the 1704 MDT volume scan of the 2 August 1981 storm. Contour intervals are 3 dB starting at 3 dB of attenuation.

be violated. Thus, in future data processing such situations will be flagged so that they will not be used in the analysis, or at least used cautiously. This can be done by flagging those areas where the S-band reflectivity is above some threshold (say 50 or 55 dBZ) and the X-band signal drops below the noise level.

4. Conclusions

An attenuation–correction scheme has been introduced for use in dual-wavelength processing. The scheme makes use of an attenuation-reflectivity relationship of the form $A = CZ^p$. Assuming a constant power, the coefficient C is found on a ray-by-ray basis, and the S-band reflectivity is used to get X-band attenuation. The scheme is not very sensitive to the choice of the power p so that one can assume it is a constant. The scheme works well under most situations, but under conditions of large hail it can lead to erroneous results because of the way the attenuation is apportioned. Thus, the scheme has been modified to help eliminate this problem.

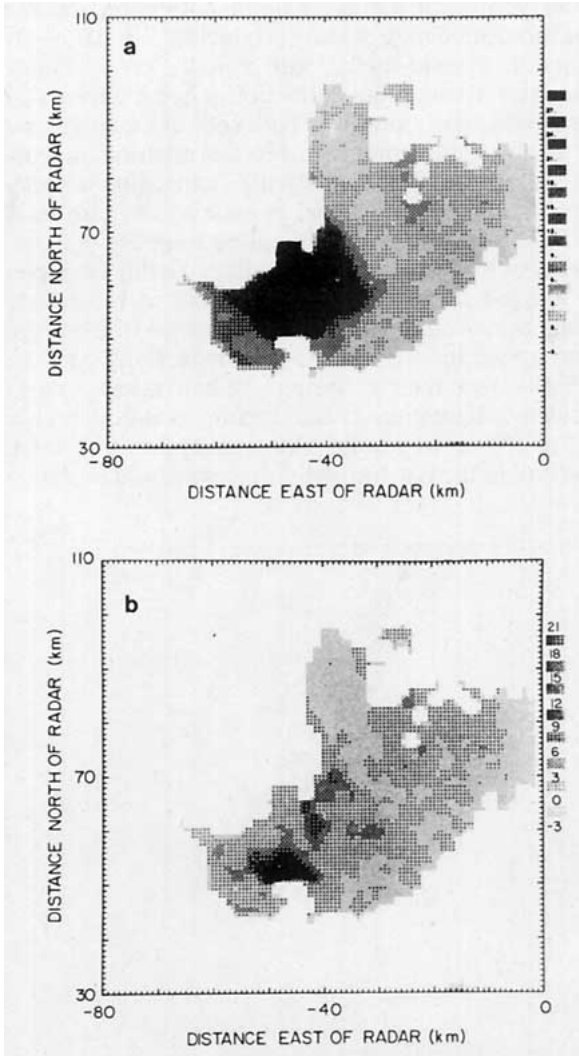

FIG. 8. Fields of dual-wavelength ratios (a) without and (b) with attenuation-correction applied for the same PPI scan shown in Fig. 2. The DWR magnitude is shown by the gray scale key on the right, starting at −3 dB and increasing at 3 dB intervals.

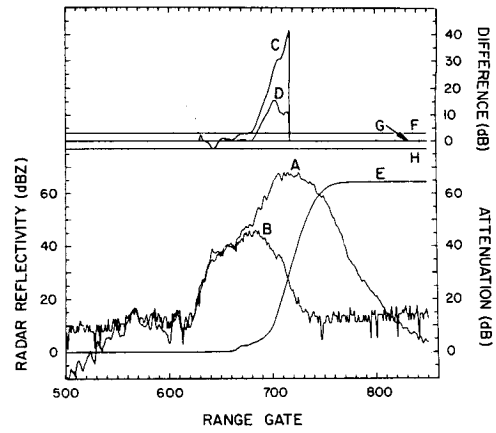

FIG. 9. An example of severe X-band attenuation along 103.75° azimuth and 0.5° elevation at 2013:32 MDT for the 11 July 1981 storm. Gate 500 is at 75 km from the radar. The labeling of the curves is the same as in Fig. 4.

The scheme is easy to use and adds relatively little extra computing time (20%) to the dual-wavelength processing. In addition the scheme works on one ray at a time as the data are read in and requires only one pass through the data. While no attenuation scheme is perfect and can handle all situations correctly, the one presented here appears to handle most situations adequately.

In this study, we used data sets coming from large, vigorous storms producing large hail and causing severe X-band attenuation. In some cases the X-band signal was attenuated so strongly that it dropped below noise level in the middle of high reflectivity cores. To use dual-wavelength radars to study such intense storms, it is probably necessary to use an S- and C-band system rather than an S- and X-band system, so that both radar signals would be able to see to the far edge.

We have shown that a vast improvement can be made in dual-wavelength analysis by using the present attenuation–correction scheme, even for a storm as strong as the 2 August storm. For average size storms, the attenuation scheme would be subjected to less strenuous conditions. In either case we feel that in dual-wavelength processing, attenuation needs to be accounted for to avoid producing erroneous positive hail signals.

Acknowledgments. We would like to express our appreciation to G. Brant Foote for his helpful comments and review of this paper. We would also like to thank Mary Davis for typing the manuscript.

REFERENCES

Atlas, D., and F. H. Ludlam, 1961: Multi-wavelength radar reflectivity of hailstorms. *Quart. J. Roy. Meteor. Soc.*, **87,** 523–534.

——, and C. W. Ulbrich, 1974: The physical basis for attenuation-rainfall relationships and the measurement of rainfall parameters by combined attenuation and radar methods. *J. Rech. Atmos.*, **8,** 275–298.

Barge, B. I., and R. G. Humphries, 1980: Identification of rain and hail with polarization and dual-wavelength radar. *Preprints 19th Conf. on Radar Meteorology,* Miami, Amer. Meteor. Soc., 507–516.

Battan, L. J., 1971: Radar attenuation by wet ice spheres. *J. Appl. Meteor.*, **10,** 247–252.

——, 1973: *Radar Observation of the Atmosphere,* University of Chicago Press, 324 pps.

Carbone, R. E., 1972: Evaluation of a dual-wavelength radar hail detector. *Preprints 15th Radar Meteorology Conf.,* Champaign-Urbana, Amer. Meteor. Soc., 7–11.

Donaldson, R. J., 1960: Thunderstorm reflectivity structure. *Preprints 8th Weather Radar Conf.,* San Francisco, Amer. Meteor. Soc., 115–125.

Eccles, P. J., 1975: Developments in radar meteorology. National Hail Research Experiment to 1973. *Atmos. Technol.*, Winter 1974–75, 34–35.

——, 1979: Comparison of remote measurements by single and dual-wavelength meteorological radars. *IEEE Trans. Geophys. Electron.*, **17,** 205–208.

Heymsfield, A. J., A. R. Jameson and H. W. Frank, 1980: Hail growth mechanisms in a Colorado storm. Part II: Hail formation processes. *J. Atmos. Sci.*, **37,** 1779–1807.

Jameson, A. R., 1977: A dual-wavelength radar study of a hailstorm. Tech. Rep. No. 39, Lab. for Atmos. Probing, Dept. of the Geophys. Sci., University of Chicago, 143 pp.

——, and A. J. Heymsfield, 1980: Hail growth mechanisms in a Colorado storm. Part I: Dual-wavelength radar observations. *J. Atmos. Sci.*, **37,** 1763–1778.

Rinehart, R. E., and J. D. Tuttle, 1981a: The effects of mismatched beam patterns on dual-wavelength processing. *Preprints 20th Conf. on Radar Meteorology,* Boston, Amer. Meteor. Soc., 676–682.

——, and ——, 1981b: A technique for determining antenna beam patterns using ground target. *Preprints 20th Conf. on Radar Meteorology,* Boston, Amer. Meteor. Soc., 672–675.

——, and ——, 1982a: Antenna beam patterns and dual-wavelength processing. *J. Appl. Meteor.*, **21,** 1865–1880.

——, and ——, 1982: Dual-wavelength processing—Some effects of mismatched antenna beam patterns. *Rad. Sci.* (in press).

Srivastava, R. C., and R. E. Carbone, 1971: The effect of signal fluctuations on the performance of dual wavelength radar hail detector. Tech. Rep. No. 20, Laboratory for Atmospheric Probing, University of Chicago, 17+ pp.

Sulakvelidze, G. K., 1965: Findings of the Caucasus anti-hail expedition (1965). [Translated from Russian by Israel Program for Scientific Translations, Jerusalem, 1967, 60 pp.]

——, 1968: VGI studies of hail-center detection. Radar Meteorology, Proc., Third All-Union Conf. [Translated from Russian by Israel Program for Scientific Translations, Jerusalem, 1971, 46–53].

Wade, C. G., 1982: A preliminary study of an intense thunderstorm which moved across the CCOPE research network in southeastern Montana. *Preprints 9th Conf. on Weather Forecasting and Analysis,* Seattle, Amer. Meteor. Soc., 388–395.